

Atmospheric Control on the Thermohaline Circulation

ARNAUD CZAJA

Department of Physics, Imperial College, London, United Kingdom

(Manuscript received 14 August 2007, in final form 23 June 2008)

ABSTRACT

In an attempt to elucidate the role of atmospheric and oceanic processes in setting a vigorous ocean overturning circulation in the North Atlantic but not in the North Pacific, a comparison of the observed atmospheric circulation and net surface freshwater fluxes over the North Atlantic and Pacific basins is conducted. It is proposed that the more erratic meridional displacements of the atmospheric jet stream over the North Atlantic sector is instrumental in maintaining high surface salinities in its subpolar gyre. In addition, it is suggested that the spatial pattern of the net freshwater flux at the sea surface favors higher subpolar Atlantic salinity, because the geographical line separating net precipitation from net evaporation is found well south of the time-mean gyre separation in the North Pacific, whereas the two lines tend to coincide in the North Atlantic. Numerical experiments with an idealized two-gyre system confirm that these differences impact the salinity budget of the subpolar gyre.

Further analysis of a coupled climate model in which the Atlantic meridional overturning cell has been artificially weakened suggests that the more erratic jet fluctuations in the Atlantic and the shift of the zero [net evaporation minus precipitation ($E - P$)] line are likely explained by features independent of the state of the thermohaline circulation. It is thus proposed that the atmospheric circulation helps “locking” high surface salinities and an active coupling between upper and deep ocean layers in the North Atlantic rather than in the North Pacific basin.

1. Introduction

The present-day ocean displays a pronounced asymmetry between the North Atlantic and Pacific basins: a vigorous meridional overturning cell couples upper and deep layers in the North Atlantic but not in the North Pacific (e.g., Ganachaud and Wunsch 2000). An explanation for this asymmetry might be that it reflects a historical accident. Deep in the past, initial conditions might have favored higher surface salinities in the North Atlantic, leading, through more likely deep convection, to formation of deep-water masses. These in turn would strengthen the meridional density gradient and drive a meridional circulation that would tend, through salt advection, to further increase the salinity of high latitudes. This positive salt feedback would be opposed by a negative temperature feedback (the heat transport associated with the overturning circulation leading to warmer high-latitude waters reducing the

meridional density gradient), as in Stommel's (1961) seminal study, resulting in a steady-state overturning circulation in the North Atlantic but none in the North Pacific.

Alternatively, one might attribute the asymmetry between North Atlantic and Pacific to the hydrological cycle and to a stronger net precipitation at high latitudes in the North Pacific than in the North Atlantic (see, e.g., a recent overview of this topic in Broecker 2005). Diagnostic studies indeed show that the net evaporation minus precipitation (hereafter $E - P$) is instrumental in lowering the salinities in the subpolar North Pacific compared to the subpolar North Atlantic (Warren 1983; Emile-Geay et al. 2003). A closer look at the differences in ($E - P$) between the two basins, however, suggest that this hydrological cycle answer is limited: the larger negative ($E - P$) over the Pacific reflects the larger rate of evaporation per unit area over the Atlantic (the precipitation rate per unit area being similar over the two basins; see Emile-Geay et al. 2003), which itself is likely due to the presence of an active overturning circulation over the Atlantic [because of the enhanced poleward heat transport associated with the latter and its driving of higher sea surface tempera-

Corresponding author address: Dr. A. Czaja, Imperial College, Prince Consort Road, Huxley Building, Room 726, London SW7 2AZ, United Kingdom.
E-mail: a.czaja@imperial.ac.uk

ture; see illustrative models of this process in Warren's (1983) study]. One is thus left with a circular chain of arguments and no clear answer as to what favors higher sea surface salinity in the North Atlantic.

It is the goal of this paper to propose that differences in the atmospheric circulation over the North Atlantic and Pacific, differences unambiguously attributable to processes independent of the state of the ocean, might be instrumental in systematically favoring the North Atlantic for higher surface salinities. In doing so, it is hoped that one can break the circular chain of arguments traditionally invoked in discussions of the dynamics of the thermohaline circulation. In essence, we propose to build upon Warren's (1983) idea that the southwest–northeast tilt of the atmospheric jet stream (and consequently the zero wind stress curl line) is key to explaining the Atlantic–Pacific asymmetry.

We start in section 2 by analyzing the time and spatial variability of the low-level winds over the North Atlantic and Pacific basins in reanalysis datasets and a control simulation of the third climate configuration of the Met Office Unified Model (HadCM3). There we show that the North Atlantic displays much more erratic north–south migrations of the westerly wind belt compared to the North Pacific. We then go on to compare the ($E - P$) pattern between the basins, with the intriguing finding that not only is the net freshening larger in the subpolar regions in the North Pacific but the zero line of the ($E - P$) field is also significantly shifted with respect to the time-mean gyre boundaries compared to the North Atlantic. The impact of these differences on the salinity budget is then investigated with an idealized two-gyre system. The model is introduced in section 3, and results of numerical experiments are presented in section 4. The role of the thermohaline circulation in setting the different behavior of the atmospheric jet stream and ($E - P$) patterns is addressed in section 5 through an analysis of a so-called hosing run with HadCM3 (Stouffer et al. 2006). Conclusions are offered in section 6.

2. The different wind and ($E - P$) fields over the North Atlantic and Pacific

a. Wind field

In Fig. 1a, we display a time-latitude contour plot of the low-level (925 mb) zonal wind, zonally averaged over a North Pacific sector (120° – 250° E). For this figure and all other observational plots in this paper, monthly data come from the National Centers for Environmental Prediction (NCEP)–National Center for Atmospheric Research (NCAR) reanalyses (Kalnay et al. 1996) over the period 1980–2005. For clarity, only

half of the record is displayed in Fig. 1. It is seen that the westerly belt oscillates in position and strength, being closer to the equator and stronger in intensity in winter, while being closer to the Pole and weaker in intensity in summer. To facilitate the analysis, a star denoting the latitude of the maximum westerly wind is superimposed for each month. The annual migration of the maximum westerly wind, hereafter referred to as the jet stream latitude Y_{JS} , is clearly seen. Over the full 26-yr record, the mean jet stream latitude is found to be $\approx 43^{\circ}$ N with a standard deviation of 3.4° .

A similar plot for a North Atlantic sector (0° – 80° W) indicates a very different situation (Fig. 1b). Much less regular displacements of the jet stream are seen: in some winters, Y_{JS} is found farther equatorward of its average summer value as in the North Pacific, but not in all. Note also the more northerly position and the wider range of latitude covered by the westerly belt over the North Atlantic compared to the North Pacific. The mean North Atlantic jet stream latitude is found to be $\approx 48^{\circ}$ N with a standard deviation of nearly 7° .

The differences in the temporal behavior of the jet stream latitude between the two ocean basins is highlighted in Fig. 2, which displays the autocorrelation function of Y_{JS} . Consistent with the annual cycle seen in Fig. 1a, the North Pacific curve (black) shows sidelobes at 6 and 12 months.¹ This is in sharp contrast with the North Atlantic (gray), for which the autocorrelation function is best described as that of a stochastic process with a short (less than a month) decorrelation time scale. In other words, if one is given the latitude of the maximum surface westerlies averaged over a given month in the North Atlantic, it is virtually impossible to predict at which latitude this maximum will be seen the following month. As we shall demonstrate in section 4, these erratic displacements of the westerly belt are particularly efficient at driving intergyre mass exchanges in the ocean through delayed expansion/contraction of the gyres, enhancing the salinity coupling between subtropical and subpolar gyres in the North Atlantic compared to the North Pacific.

b. ($E - P$) pattern

We present in Fig. 3a the long-term-mean low-level (925 mb) zonal wind (contours) superimposed on the long-term-mean net ($E - P$; shading). It is seen that in the Atlantic, the largest zonal winds are found where, in the mean, the ($E - P$) field vanishes (the line separat-

¹ Note that the results are unchanged if the Pacific calculation is repeated with its western (120° – 180° E) or eastern (180° – 250° E) domains only (not shown).

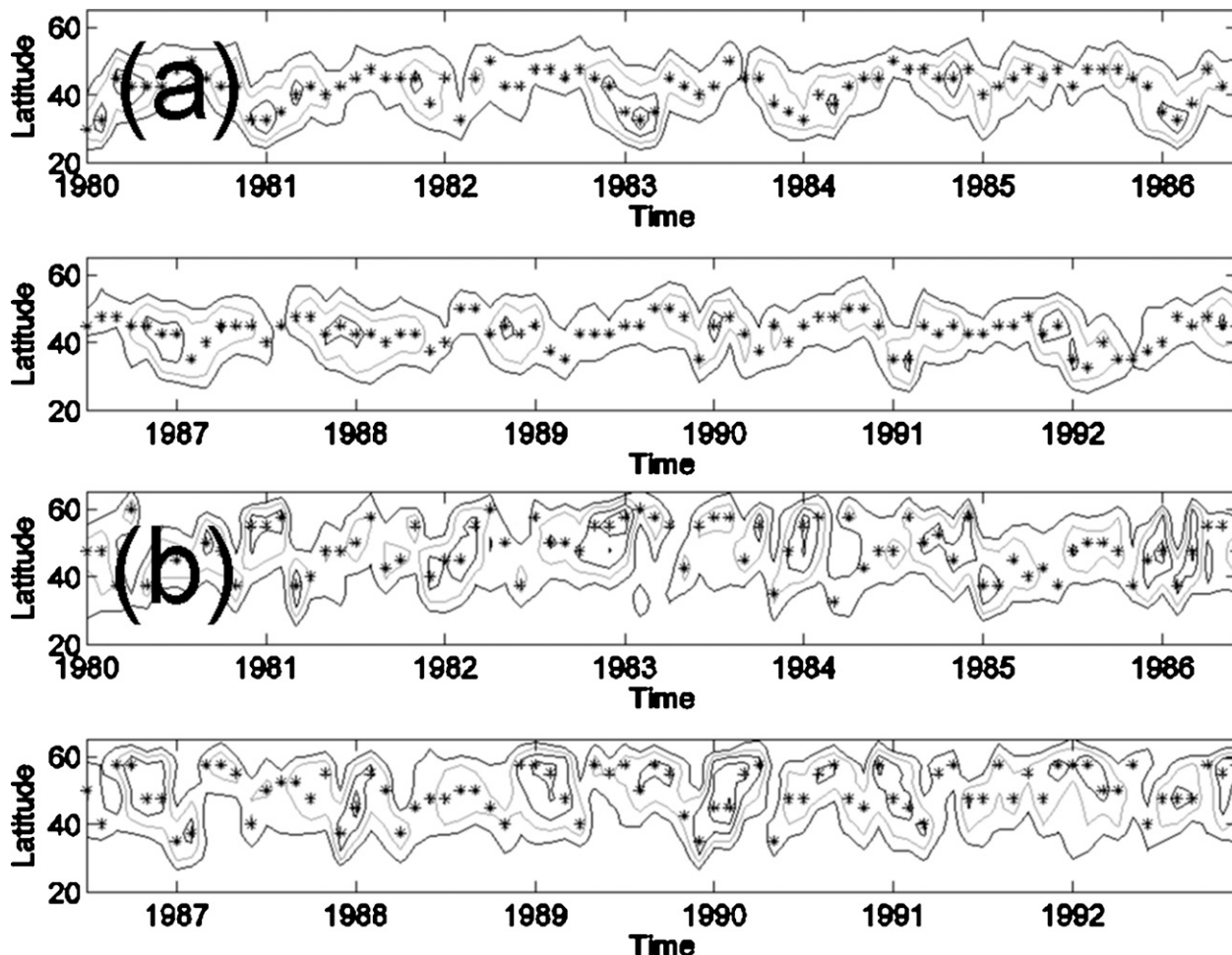


FIG. 1. (a) Lat–time contours of westerly wind at 900-mb contour interval ($CI = 2.5 \text{ m s}^{-1}$ with the 5 m s^{-1} contour highlighted in gray), zonally averaged over a North Pacific sector (120° – 250°E). The year on the x axis refers to the month of January. The star indicates for each month the latitude of the maximum westerly wind. Monthly data from the NCEP–NCAR reanalyses. (b) Same as Fig. 1a, but for a North Atlantic sector (0° – 80°W).

ing net precipitation from net evaporation is highlighted as a continuous bold line in Fig. 3a). In the North Pacific, however, the belt of maximum westerlies is found farther poleward of the line separating net mean evaporation and precipitation. As a result, a Sverdup ($1 \text{ Sv} \equiv 10^6 \text{ m}^3 \text{ s}^{-1}$) transport calculation (Fig. 3b) indicates that the line separating the ocean-mean gyres (bold dashed line in Fig. 3b—essentially set by the location of maximum westerlies) coincides with the zero ($E - P$) line in the North Atlantic, but not in the North Pacific. It is readily expected that this state of affairs will tend to reduce the salinity of the subpolar gyre in the North Pacific compared to the North Atlantic because water parcels advected into the subpolar gyre from the subtropical gyre will have experienced more freshening in the Pacific than in the Atlantic. This will be confirmed through idealized model experiments in section 4.

To gain insight into the mechanisms responsible for this ($E - P$) pattern difference we display in Fig. 4 the seasonal ($E - P$) pattern (shading) superimposed on the 925-mb zonal winds (contours), in a format similar to Fig. 3a. In both boreal winter (Fig. 4a) and summer (Fig. 4b), the North Atlantic shows largest zonal winds over the line separating net precipitation from net evaporation (bold black line). In contrast, in the North Pacific, winter and summer differ: largest zonal winds are found over the zero ($E - P$) line in winter (as in the Atlantic), but not in summer, during which the largest winds are found north of the zero ($E - P$) line. This is understandable considering the large moisture input from lower latitudes by the East Asian monsoon to the North Pacific during boreal summer (Emile-Geay et al. 2003). In wintertime, however, the North Atlantic and Pacific moisture fluxes reflect the activity of midlatitude storms with an in-phase relationship between low-

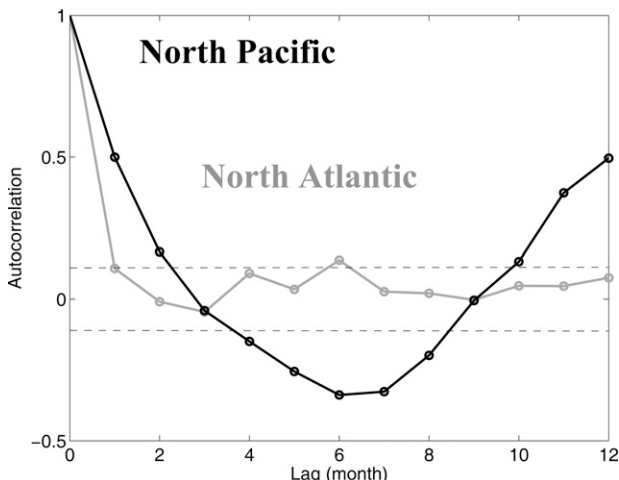


FIG. 2. Autocorrelation function (lag in month) of the jet position for the North Atlantic (gray) and Pacific (black). The dashed line indicates a 95% confidence level, assuming all months are independent.

level winds and moisture fluxes. This spatial relationship holds in the North Atlantic in summer, reflecting the absence of a significant basin-scale monsoonal circulation over this basin in boreal summer.

c. Coupled model results

The previous dataset analysis is suggestive, but considering the uncertainties in the reanalysis estimates of surface evaporation, precipitation, and wind stress, its application to a “freely running” (i.e., nonflux adjusted) coupled climate model is warranted. We have thus analyzed the control simulation of HadCM3 (see Gordon

et al. 2000 for an overview of the model climatology) in a similar way as we did for the reanalysis data.

Figure 5a shows, in a format similar to Fig. 3b, the mean Sverdrup streamfunction and the $(E - P)$ from a monthly climatology constructed over the model years 1959–2199. Compared to its observational counterpart (Fig. 3b), there is now less agreement between the position of the gyre separatrix (heavy dashed line) and that of the zero $(E - P)$ line (heavy continuous) over the North Atlantic. Indeed, net precipitation is seen clearly over the northern rim of the model Atlantic subtropical gyre. Nevertheless, compared to the North Pacific, the incursion of the region of net precipitation is less pronounced in the North Atlantic than it is in the North Pacific. The zero $(E - P)$ line is seen to tilt strongly in a northeast–southwest direction, reaching equatorward of the gyre center in the North Pacific, but it is only confined to regions of weak anticyclonic flow, poleward of the gyre center in the North Atlantic. (To be more quantitative, about 40% of subtropical gyre gridpoints experience net precipitation in the North Pacific, whereas 25% do in the North Atlantic.) Further analysis, stratified by seasons, confirms that the larger incursion of the region of net precipitation in the North Pacific is a result of the large impact of the summer monsoon in the North Pacific (not shown). Thus, in HadCM3 as in reanalysis data, the $(E - P)$ pattern will tend to freshen a larger portion of the subtropical gyre in the North Pacific than in the North Atlantic.

Next we turn to the investigation of jet stream behavior and display in Fig. 6 the result of the “jet tracking” procedure described in section 2a for the reanaly-

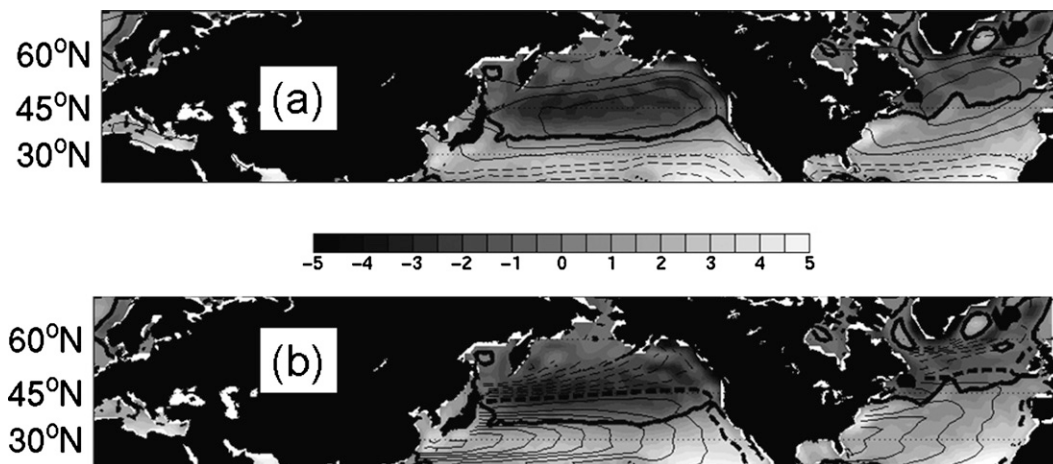


FIG. 3. Annual mean net surface freshwater flux (shading, in units of $10 \mu\text{kg s}^{-1} \text{m}^{-2}$) and (a) 925-mb zonal winds ($\text{CI} = 2 \text{ m s}^{-1}$, dashed when westward) and (b) Sverdrup transport streamfunction ($\text{CI} = 10 \text{ Sv}$, 1) computed from wind stress curl, assuming no transport at the eastern boundary of each basin. The heavy continuous black line in both panels is the 0 line of the freshwater flux (north of it, net precipitation; south of it, net evaporation), while in (b), the dashed black line is the 0 of the Sverdrup streamfunction. All data used are taken from the NCEP–NCAR reanalysis over the 1980–2005 period.

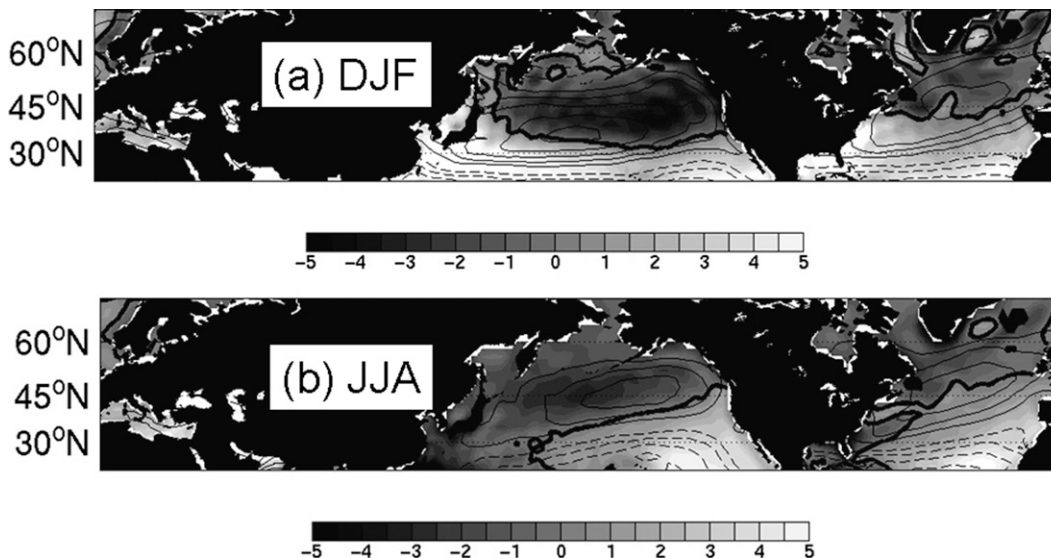


FIG. 4. Same as Fig. 3a, but for seasonal averages: (a) December to January and (b) June to August.

sis data but now applied to a 20-yr slice of the HadCM3 control run. As was found in the reanalysis data (Fig. 2), the Atlantic jet position is quickly decorrelated, while a clear seasonal cycle is seen for the North Pacific jet (Fig. 6, gray and black continuous curves, respectively).

In summary, reanalysis data and coupled model outputs both suggest that the atmospheric jet stream and associated $(E - P)$ field display striking differences between North Atlantic and Pacific: (i) a model for the westerly belt position over the North Pacific should, to zero order, include a harmonic displacement, whereas such a model would best be chosen as random meridional excursions over the North Atlantic, and (ii) an idealized distribution of $(E - P)$ should take into account the pronounced shift in gyre boundary and the

zero $(E - P)$ line in the North Pacific. We now investigate in an idealized two-gyre system whether these differences in atmospheric forcing impact the surface salinity distribution of the gyres. Whether the term “atmospheric forcing” is appropriate, that is, whether the oceanic circulation itself determines the differences in wind/ $(E - P)$ structure between the North Atlantic and Pacific will be discussed in section 5.

3. A kinematic model for the salinity of a two-gyre system

a. Model description

We consider a column of water extending from the sea surface to the base of the mixed layer. The column is advected by a prescribed geostrophic flow (2D, non-

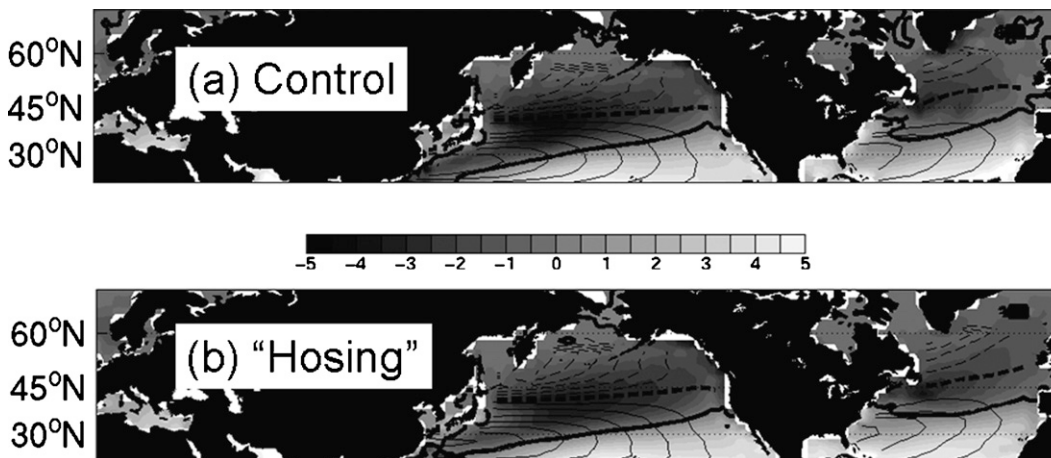


FIG. 5. Same as Fig. 3b, but for HadCM3 (a) control and (b) hosing experiments.

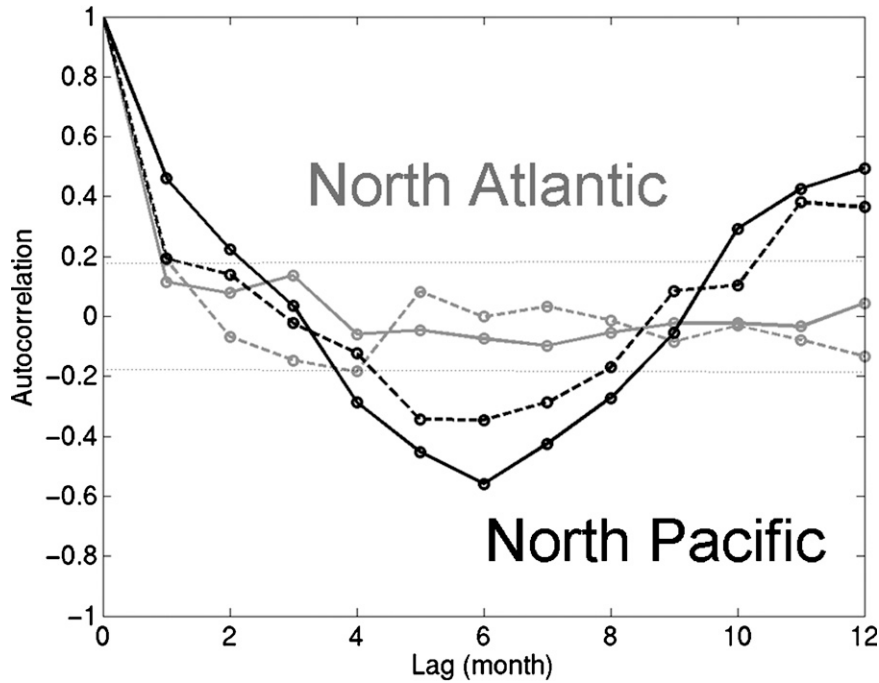


FIG. 6. Same as Fig. 2, but for HadCM3. Autocorrelation functions from the control experiment (years 2200–19) are plotted in continuous lines, while those from the hosing experiment (years 90–110) are plotted in dashed lines.

divergent) and changes its salinity through evaporation and precipitation at the sea surface. Denoting the Lagrangian derivative by d/dt , the trajectory and salinity budget of the column reads,

$$\frac{dx_c}{dt} = u_g, \tag{1}$$

$$\frac{dy_c}{dt} = v_g, \tag{2}$$

$$\frac{ds_c}{dt} = \frac{s_o}{\rho_o h} (E - P), \tag{3}$$

in which t is time, (x_c, y_c, s_c) denote the west–east, south–north position and salinity of the column, (u_g, v_g) denote the zonal and meridional geostrophic velocities, P and E are the precipitation and evaporation rates per unit area ($\text{kg s}^{-1} \text{m}^{-2}$), h is the mixed layer thickness, and s_o, ρ_o are reference (constant) salinity and density, respectively.

For a given $(E - P)$ forcing and prescribed (time dependent) geostrophic flow, a steady-state salinity field can be achieved if water parcels typically experience on average as much evaporation as precipitation along their trajectories. For a “North Atlantic configuration,” in which the zero $(E - P)$ line and the time-mean gyre boundary are close to one another,

Lagrangian intergyre mass exchange will thus be the key to reaching the steady state. Alternatively, in an Eulerian view, this is equivalent to saying that correlation between velocity and salinity, that is, the rectified salt flux at the time-mean subtropical/subpolar gyre boundary ($[v_g^* s^*]$ term, in which $[\]$ and $*$ denote the zonal average over the basin and the deviation from it, respectively) opposes the $(E - P)$ forcing. We emphasize that if Lagrangian techniques are often used in studies of temporal salinity variations (e.g., Spall 1993; Mignot and Frankignoul 2004), our focus here is on the time-mean salinity distribution.

The model (1)-(2)-(3) is clearly very simplified. First, it does not take into account the role of Ekman currents nor entrainment processes on the mixed layer salinity budget. This is an issue, considering that the time-mean Ekman salt transport at the intergyre boundary is a significant term in the salinity budget of the gyres’ mixed layer (a scaling readily suggests that $v_{\text{Ek}} \partial s / \partial y$ in which v_{Ek} is the time-mean Ekman current and s is the time-mean salinity of the mixed layer, is of the same order of magnitude as the $E - P$ forcing when evaluated at the intergyre boundary). Nevertheless, we wish to assess the impact of North Atlantic–North Pacific differences in wind variability rather than time-mean winds on the surface salinity budget. As a result, the relevant Ekman salt flux is the rectified salt flux (cor-

relation between Ekman current and salinity anomalies), which we expect to be weaker than the rectified geostrophic salt flux in the mixed layer, especially as the time scales considered increase [hint of this is provided in the study by Mignot and Frankignoul (2003), who showed that salinity anomalies become increasingly controlled by geostrophic rather than Ekman advection as the time scale considered increases]. Second, and maybe more importantly regarding the larger issue of the thermohaline circulation, the model only represents the mixed layer and omits completely the role of intermediate layers on the salinity budget. Considering the emphasis of the literature on the Atlantic basin salinity budget as a whole (upper, intermediate, and deep layers as well as the South and North Atlantic), as well as interbasin exchange of salty intermediate waters (South Atlantic, Bering Strait, and Mediterranean outflow) when discussing the stability of the thermohaline circulation (e.g., Rahmstorf 1996; Weijer et al. 1999; Vellinga et al. 2002), this is an important limitation of our study. Nevertheless, as far as we are aware, it is the first time that the impact of strikingly differing atmospheric jet stream variability (North Atlantic versus Pacific; see section 2) on the dynamics of the thermohaline circulation is investigated. For this reason, we feel justified in starting with the most elementary model.

b. The geostrophic flow

The geostrophic velocities are prescribed through a streamfunction ψ_g ,

$$\psi_g(x, y, t) = \psi_{\max} \sin\left(\frac{\pi x}{L_x}\right) \sin\left(\frac{2\pi y}{L_y}\right) + \delta\psi(t) \sin\left(\frac{\pi x}{L_x}\right) \sin\left(\frac{\pi y}{L_y}\right), \quad (4)$$

in which (L_x, L_y) are the zonal and meridional domain size, respectively, and (x, y) denote Cartesian zonal and meridional coordinates. The geostrophic streamfunction (4) is the sum of a simple time-mean two-gyre system streamfunction (first term on the rhs), with peak amplitude scaled by $(\psi_{\max} > 0)$, and a time dependent part (second term on the rhs). The latter is at maximum at the intergyre boundary and, when positive, represents an expansion of the subtropical gyre. Conversely, when negative, it represents an expansion of the subpolar gyre. The strength of this anomalous “intergyre gyre” is measured by $\delta\psi(t)$.

The intergyre gyre is meant to represent the oceanic response to time-dependent meridional excursions of the atmospheric jet stream discussed in section 2. When

the jet is in a more poleward position than on average, the region of anticyclonic wind stress curl forcing expands and that of positive wind stress curl shrinks. If this forcing is represented as a single fixed spatial pattern of anomalous wind stress curl with a time-dependent amplitude, we expect the linear (Sverdrupian) response of the ocean to consist of an anomalous streamfunction whose pattern straddles the zero line of the time-mean two-gyre system, as modeled by (4)—see the studies by Marshall et al. (2001) and Czaja and Marshall (2001) for a discussion of the intergyre gyre dynamics in the context of the response of the ocean to North Atlantic Oscillation forcing.

The intergyre gyre is further decomposed as

$$\delta\psi(t) = a\psi_{\max}\phi(t), \quad (5)$$

in which a is a nondimensional parameter controlling the relative strength of the intergyre gyre compared to the mean gyre, and the time behavior of $\delta\psi$ is described by the (nondimensional) function $\phi(t)$. The latter will be prescribed as either harmonic at the annual period (with the North Pacific in mind) or stochastic (with the North Atlantic in mind); we will consider both the fast response to the winds [i.e., a white spectrum for $\phi(t)$ on time scales longer than a month] and the slower response with a red spectrum down to time scales of order of a decade and a flat spectrum on longer time scales. This rationale is motivated by the linear theory of the response of a midlatitude (flat bottom) gyre to stochastic wind forcing (e.g., Frankignoul et al. 1997), associating the fast and slow intergyre gyres with barotropic and baroclinic dynamics, respectively.

The prescribed geostrophic flow is purely large scale and no efforts have been made to include a representation of mesoscale eddies, as has been done in a similar kinematic context by Yang (1996). This might seem at first sight surprising, considering that the intergyre boundary is a region of intense eddy activity. Our rationale is twofold. First, as far as the upper ocean layers are concerned, several studies suggest only a weak mesoscale eddy material transport across the gyres. Berloff et al. (2002), in an idealized quasigeostrophic model at large Reynolds number with steady winds, show that typically a few percent, at most, of “fluid parcels” initially released in the subtropical gyre are able to reach the subpolar gyre over a time scale of 500 days (about 250 eddy advective time scales for an eddy length scale of 100 km and velocity of 50 cm s^{-1}). The results to be discussed below indicate that a fraction of order one of such parcels is transported to the subpolar gyre by the large-scale eddies (the anomalous intergyre gyre) over a few intergyre advective time scales (a few decades).

This appears consistent with the observations by Bower and Lozier (1994) of weak (mesoscale eddy) cross-gyre transport in upper layers of the Gulf Stream. Second, in the presence of imposed changes in large-scale winds, there is a strong coupling between resulting changes in large and mesoscale circulations (e.g., Rhines and Schopp 1991; Dewar 2003). Dewar (2003), for instance, recently showed how anomalies in Ekman pumping akin to those driving the anomalous intergyre gyre in Eq. (4) have a complex impact on the structure of the oceanic variability (itself resulting from two-way interactions between the mesoscale and the large-scale flow) in an idealized quasigeostrophic model. Rather than attempting to parameterize such difficult coupling, and considering the possible weakness of cross-gyre mesoscale transport in upper layers, we have opted for the simple solution of solely including large-scale geostrophic flows.

c. Key model parameters

A natural time scale in this problem is the advective time scale τ_{adv} , the typical time it takes a column to circulate around the subtropical or subpolar gyre:

$$\tau_{adv} = \frac{L_x L_y}{\psi_{max}}. \tag{6}$$

For both the North Atlantic and the North Pacific, this time scale is of the order of a decade, and we set $\tau_{adv} = 10$ yr in the following. [From Sverdrup balance, the geostrophic streamfunction is expected to increase linearly with zonal basin size, assuming no x dependence in the wind stress, so that the ratio (6) does not change, even though L_x is larger in the Pacific.]

A second time scale τ_{forc} is introduced by the freshwater forcing. Denoting by F_o the typical scale of the freshwater forcing ($E - P$), τ_{forc} is the time it takes to “empty” a mixed layer column through net evaporation:

$$\tau_{forc} = \frac{\rho_o h}{F_o}. \tag{7}$$

For typical values $h = 100$ m and $F_o = 3.10^{-5}$ kg s⁻¹ m⁻², we find $\tau_{forc} \approx 100$ yr [equivalently, through (3), a typical salt tendency is $s_o/\tau_{forc} = 35/100$ yr ≈ 0.3 psu yr⁻¹].

Introducing the nondimensional variables (denoted by a prime) $x = L_x x'$, $y = L_y y'$, $t = \tau_{adv} t'$, $s = s_o s'$ and $(E - P) = F_o (E - P)'$, the system (1)-(2)-(3) is rewritten as, using (4) and (5),

$$\begin{aligned} \frac{dx'}{dt'} &= -2\pi \sin(\pi x') \cos(2\pi y') \\ &\quad - \pi a \phi(t') \sin(\pi x') \cos(\pi y'), \end{aligned} \tag{8}$$

$$\frac{dy'}{dt'} = \pi \cos(\pi x') \sin(2\pi y') + \pi a \phi(t') \cos(\pi x') \sin(\pi y'), \tag{9}$$

$$\frac{ds'}{dt'} = \frac{\tau_{adv}}{\tau_{forc}} (E - P)'. \tag{10}$$

The three controlling parameters are readily seen from (8)-(9)-(10), namely, the ratios a and $\tau_{adv}/\tau_{forc} \ll 1$ (as implied by the above scalings), and from the form of the time-dependent function $\phi(t')$. The amplitude parameter a is typically smaller than unity for realistic oceanic conditions. Indeed, for the particular form of forcing considered in (4), a value $a = 0.6$ is associated with a shift of the intergyre boundary by $\Delta y' = \pm 0.1$ (about $\pm 4^\circ$ latitude for a two-gyre system of 4000-km meridional extent): observed Gulf Stream shifts are observed to be at most a couple of degrees of latitude (e.g., Frankignoul and de Coëtlogon 2001).

4. Model results

Our strategy is to investigate separately the effects that different winds and different ($E - P$) patterns have on the subpolar gyre salinity budget. To address the role of the winds (section 4a), we will consider a non-forced initial value problem ($E - P$ set to 0), in which the subpolar gyre salinity is initially lowered compared to the subtropical salinity, and we will investigate how efficiently expansions/contractions of the gyres establish an equilibrium salinity distribution. In these experiments, the control parameter will be the form of $\delta\psi(t)$, that is, both a and the time behavior of ϕ (harmonic or stochastic). To address the role of the differing ($E - P$) pattern (section 4b), we will study a forced problem using the shift between the zero ($E - P$) line and the time-mean gyre boundary as the sole control parameter.

a. Atlantic versus Pacific: Role of wind fluctuations

We consider a simple relaxation experiment: assume that at $t = 0$, the subtropical gyre salinity is set to $s = 35$ psu and that of the subpolar gyre at $s = 33$ psu. For $t > 0$, we allow expansion/contraction of the two-gyre system and measure as a function of time the salinity contrast between the gyres by averaging the salinity of columns present in each gyre (1000 columns were used for this purpose; see the appendix for details of the numerical calculations).

As an idealization of the North Pacific wind forcing, we consider the following model for the intergyre gyre strength:

$$\phi(t') = \sqrt{2} \cos(\omega_{\text{yr}} t'), \quad (11)$$

in which $\omega_{\text{yr}} = 2\pi\tau_{\text{adv}}/1 \text{ yr}$ is the nondimensional annual angular frequency. The resulting time evolution of the salinity contrast between the gyre is displayed in Fig. 7 (black curve) for $a = 0.5, 0.3, 0.1$. Even for unrealistically large amplitude expansions/contractions of the gyre ($a = 0.5$; Fig. 7a), the salinity relaxation is weak, dropping by less than 30% (0.6 psu) in 20 advective time scales (i.e., about 200 yr).

To compare this result to an Atlantic configuration, we have considered the following idealization of the North Atlantic wind forcing:

$$\phi(t') = \zeta(t'), \quad (12)$$

in which ζ is a Gaussian white noise with unit variance. The function ζ was chosen such that the decorrelation time scale of the intergyre gyre is smaller than 6 months (see the appendix for details of the numerical procedure). Forty relaxation experiments, with different wind history and different initial conditions for ϕ , were conducted, all of which are shown in Fig. 7 (gray curves), for the same values $a = 0.5, 0.3, 0.1$. [Note that the factor $\sqrt{2}$ in (11) is included so that the variance of $\delta\phi$ is the same in the harmonic and stochastic cases]. It is clear that for comparable amplitudes (i.e., same variance), stochastic wind forcing (gray curves) drives a much more efficient mass exchange between gyres than an annual wind forcing (black curve).

The harmonic case discussed here for the North Pacific has been studied intensively in other studies in relation to chaotic advection problems. Bowman and Cohen (1997) considered a model very similar to ours in the context of the interhemispheric mass exchange induced by seasonal modulation of the Hadley circulation. In this atmospheric context, the advective time scale is smaller than a year and the perturbations in the shape of the Hadley cell are strong ($a \geq 1$). In this different regime of parameters, a large impact of seasonal expansion/contraction was obtained. Liu and Yang (1994) also considered a model similar to our Pacific configuration, this time with oceanic applications in mind. They showed that the chaotic advection mechanism works best for harmonic expansion/contraction with a period slightly smaller than the advection time scale (about 5 yr) and relatively large amplitude. At higher frequency or smaller amplitude, chaotic advection was weak, in agreement with the results presented here.

The North Atlantic case illustrated in Fig. 7, in which

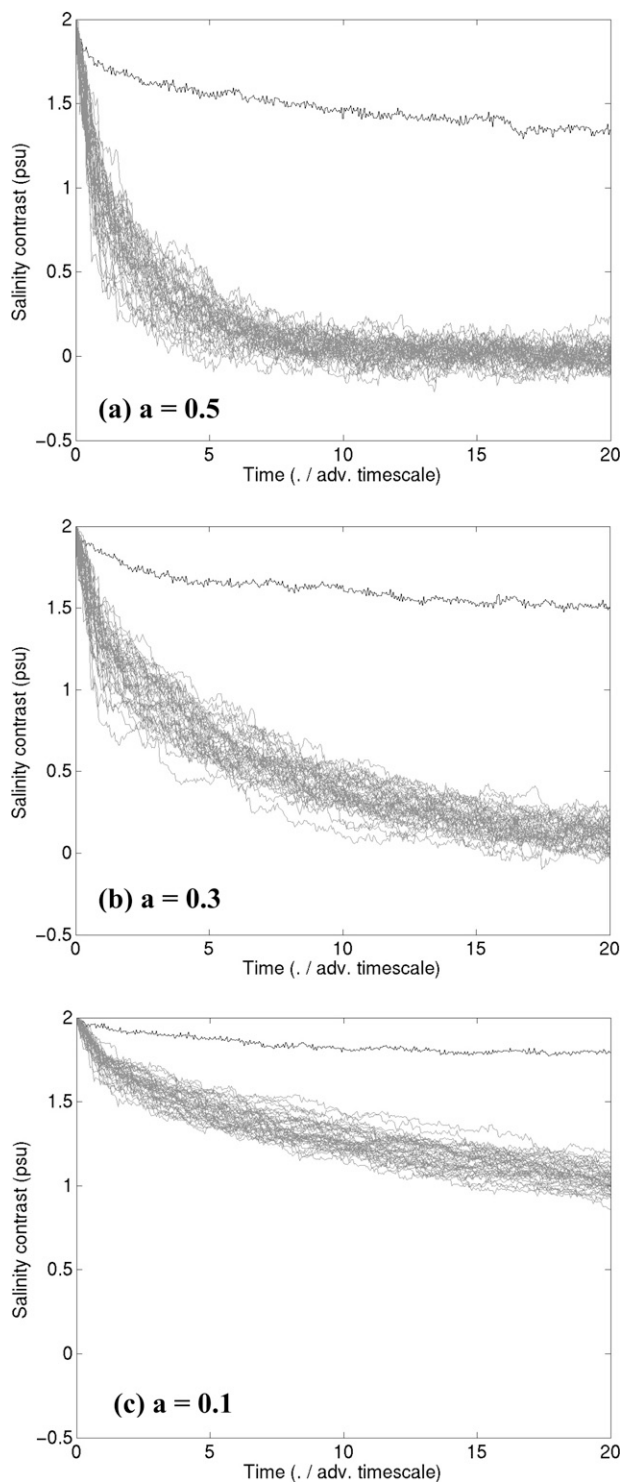


FIG. 7. Salinity relaxation experiments. Evolution of the salinity contrast (psu) across the gyres as a function of time (normalized by the advective time scale ≈ 10 yr) for the harmonic (black curve) and stochastic (gray) forcings: (a) $a = 0.5$, (b) $a = 0.3$, (c) $a = 0.1$.

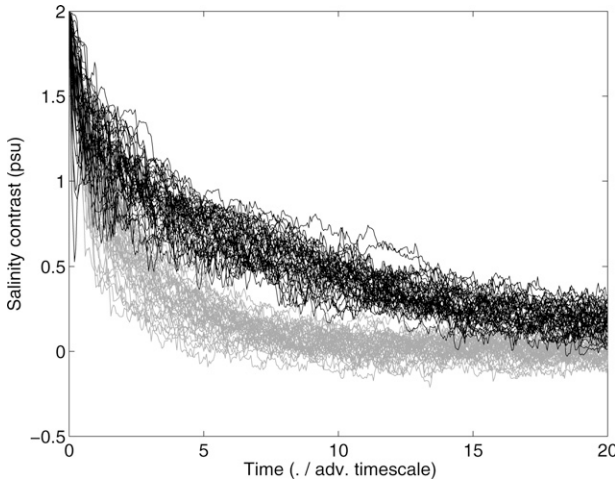


FIG. 8. Same as Fig. 7a, but for short (same gray curves as in Fig. 7a) and long memory (black curves) intergyre gyres.

the anomalous intergyre gyre is treated as a white noise on time scales beyond a few months (gray curves), is particularly efficient at relaxing the salinity contrast between the gyres. If such a quick decorrelation time is expected from the barotropic mode, a much larger decorrelation time is expected for a baroclinic intergyre gyre. Indeed, linear theory predicts the decorrelation time of the latter to be the time it takes for long baroclinic Rossby waves to cross the basin from east to west (Frankignoul et al. 1997)—the time being, in midlatitudes, of the same order as the advective time scale. We thus have considered another stochastic model for the North Atlantic, namely,

$$\phi(t') = \chi(t'), \tag{13}$$

in which $\chi(t')$ is a random variable of unit variance with an exponential autocorrelation function and a decorrelation time scale equal to τ_{adv} (a first-order Markov process was used for this purpose). Figure 8 compares 40 relaxation experiments for the rapidly (gray) and slowly (black) decorrelated intergyre gyre models (12) and (13), respectively, both with $a = 0.5$. It is seen that the increased memory of the intergyre gyre decreases its efficiency at exchanging fluid parcels between subtropical and subpolar gyres, even though the relaxation is still stronger than in the harmonic case (cf. Fig. 7a). The reason for this is simple: as the memory of the intergyre gyre becomes comparable to the advective time scale, shear dispersion within a gyre (akin to that described by Rhines and Young 1983) destroys the correlation between the salinity of columns and their meridional displacement. As a result, the salt flux across the time-mean intergyre gyre boundary ($y' = 0.5$) is reduced and the relaxation of the salinity contrast becomes weak. Additional experiments, not presented

here, in which the intergyre gyre anomaly is kept fixed in time show this process clearly: for an expansion of the subtropical gyre, for example, a large salt flux is produced initially as fresh columns move south on the eastern side of the basin and salty columns move north on the western side, but the salt flux reverses sign at $t' \approx 1$ as the fresh column now moves northward and the salty ones southward. On longer time scales, shear dispersion removes any correlation between the salinity of columns on the west and east sides of the basin and the salt flux is essentially zero (not shown).

In summary, the irregular nature of the fluctuations in the location of the atmospheric jet over the North Atlantic is instrumental in increasing the exchange of fluid parcels between subtropical and subpolar gyres in this basin. A much weaker role of wind forcing is instead suggested in the North Pacific.

b. Atlantic versus Pacific: Role of (E - P) pattern

To account for the shift between the zero ($E - P$) line and the time-mean gyre separatrix, a nondimensional parameter f_{asym} is introduced in the definition of the idealized ($E - P$) forcing pattern,

$$(E - P)' = \begin{cases} -1 & \text{for } y' > 1 - f_{asym} \\ f_{asym}/(1 - f_{asym}) & \text{otherwise} \end{cases} \tag{14}$$

For a symmetric ($E - P$) forcing ($f_{asym} = 1/2$), which we choose as representative of the North Atlantic, Eq. (14) represents equal net evaporation and precipitation over the time-mean subtropical and subpolar gyres, respectively. For the North Pacific, a value $f_{asym} = 0.6$ is chosen, so that the strength of the net precipitation is unchanged over the time-mean subpolar gyre ($y' > 1/2$), but the time-mean subtropical gyre experiences net precipitation on its northern rim ($0.5 > y' \geq 1 - f_{asym} = 0.4$) and net evaporation for $y' \leq 1 - f_{asym} = 0.4$.

It is clear that if the strength of the net evaporation is the same in the Atlantic and Pacific configurations, the salinity of subtropical fluid parcels making frequent excursions into the subpolar gyre will be lower in the Pacific than in the Atlantic configuration (the averaged evaporation over the subtropical gyre would be reduced and, in addition, the region close to the time mean gyre boundaries, from which those parcels more frequently originate, would experience net freshening). This would lead us straight to the conclusion that the differing ($E - P$) patterns favor the North Atlantic for higher subpolar salinities. To make a more stringent comparison, and considering furthermore that an equilibrium could not be maintained in this situation (the North Pacific basin as a whole would then experience

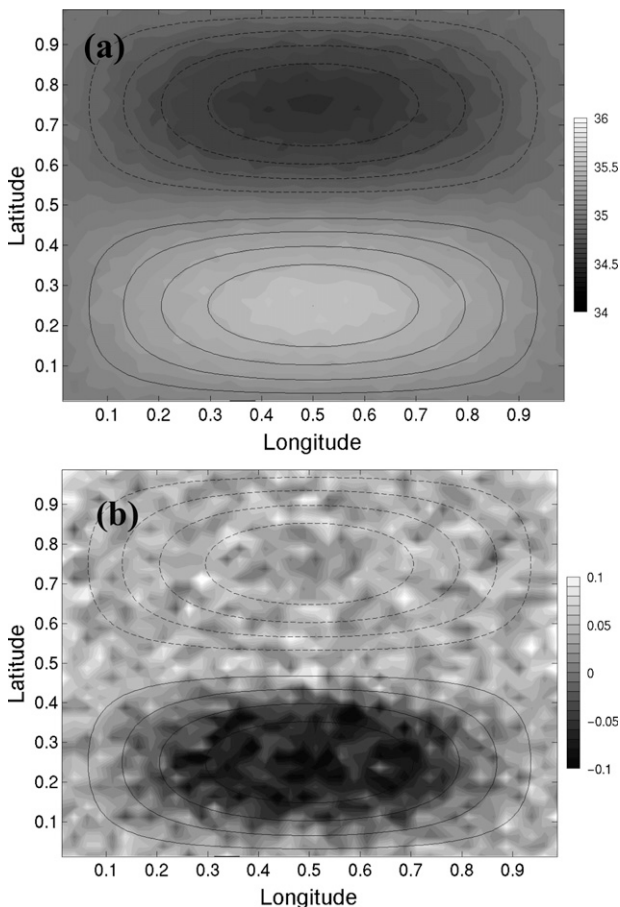


FIG. 9. Time-mean salinity (psu, shading) and geostrophic streamfunction (contours) for (a) Atlantic experiment and (b) Atlantic minus Pacific.

net precipitation), we have increased the strength of the net evaporation by a factor $f_{\text{asym}}/(1 - f_{\text{asym}})$ over the southern Pacific subtropical gyre so that both the Atlantic and Pacific basins as a whole do not experience net freshening or net evaporation. Despite this increased evaporation in the North Pacific configuration, we show below that higher salinities are found in the North Atlantic subtropical gyre.

The time-mean distribution of salinity for the North Atlantic case ($f_{\text{asym}} = 1/2$) is shown in Fig. 9a, for a simulation using model (12) with $a = 0.5$ and a freshwater forcing $\tau_{\text{adv}}/\tau_{\text{forc}} = 0.1$. The only difference between the North Atlantic and Pacific configuration is thus the $(E - P)$ field. One thousand Lagrangian columns were followed over 200 advective time scales and the time mean was computed over the last 50 advective time scales of an ensemble of 10 simulations. Time series of salinities at fixed locations indicate that a mean state is achieved over 10–20 advective time scales (not shown), in agreement with Fig. 7a. The expected low

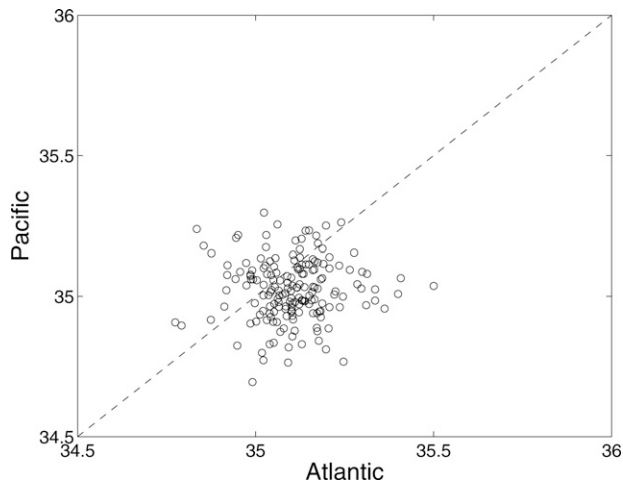


FIG. 10. Scatterplot of the salinity s_{stg} (psu) of subpolar gyre columns when last in the subtropical gyre (horizontal axis = Atlantic, vertical axis = Pacific, the dashed line indicating when the two basins' salinity are equal).

subpolar and high subtropical salinities are seen, with a salinity contrast on the order of 1 psu between the gyres.

The difference between the North Atlantic and North Pacific cases is shown in Fig. 9b. As expected from the larger subtropical net evaporation in the Pacific case, salinities are lower at the core of the subtropical gyre in the North Atlantic than in the Pacific (dark shading). Over the subpolar gyre, though, where the net freshening is *the same* between the basins, higher salinities are seen in the North Atlantic by typically 0.1 psu (light shading). One also notices higher Atlantic subtropical salinities along the rim of the subtropical gyre core. This is a direct consequence of the strip of net freshening over the northernmost Pacific subtropical gyre: columns frequently exchanged with the subpolar gyre originate from this strip and display figure-eight-like trajectories around the gyres.

Because the prescribed geostrophic velocities are statistically identical in the Atlantic and Pacific configurations [only the pattern of $(E - P)$ forcing is altered here], the higher subpolar Atlantic salinities must originate from the higher salinity of columns entering its subpolar gyre from the subtropics. To check this, we have focused on a region at the core of the (time mean) subpolar gyre ($0.3 \leq x' \leq 0.7$ and $0.65 \leq y' \leq 0.85$) and assessed the typical salinities of columns, “ventilating” this region from the subtropics. At a given time, we have considered every column within this box and computed its salinity s_{stg} at the time it was last in the (time mean) subtropical gyre. A scatterplot of s_{stg} computed for the North Atlantic and Pacific cases is shown in Fig. 10, each circle representing an estimate of s_{stg} at a time

$150 \leq t' \leq 200$ (the estimate was computed at every advective time scale within this interval so 51 circles are shown). It is seen that the North Atlantic subpolar gyre is ventilated by columns of subtropical origins with salinities typically higher by 0.1 psu compared to their Pacific equivalent, in agreement with the salinity contrast shown in Fig. 9b. In Fig. 10, about 65% of the circles lie in the domain $s_{\text{stg}}(\text{Atlantic}) > s_{\text{stg}}(\text{Pacific})$.

In summary, at fixed and equal intergyre mass exchanges, the shift of the zero ($E - P$) line with respect to the time-mean gyre boundary is instrumental in favoring higher surface salinities in the North Atlantic subpolar gyre compared to the Pacific. Considering that the intergyre mass exchange is itself stronger in the North Atlantic than in the North Pacific (section 4a), the results presented in section 4 add constructively to suggest that differences in atmospheric circulation exert a control on the location of the oceanic basin, developing high subpolar gyre salinity and, possibly, an overturning circulation.

5. Thermohaline circulation impact on North Atlantic and Pacific meteorology

We now turn to the issue regarding the role of the thermohaline circulation in possibly setting the differences in jet stream behavior and ($E - P$) patterns discussed in section 2. To do so, we present the results of an analysis of a so-called hosing run with HadCM3, in which a “collapse” of the Atlantic overturning streamfunction results from an externally imposed strong freshwater flux anomaly at high latitudes. In such a setting, changes in atmospheric circulation can uniquely be attributed to changes in ocean circulation driven by the freshwater flux anomaly, so that the hosing experiment provides a useful tool to address this question (causes and effects would be much harder to disentangle in the control run of HadCM3).

The particular experiment considered is the 1 Sv ($1\text{Sv} \equiv 10^6 \text{ m}^3 \text{ s}^{-1}$) hosing experiment, in which a uniform freshwater flux anomaly of 1 Sv is imposed over the North Atlantic ($50^\circ\text{--}70^\circ\text{N}$) for 100 yr and then turned off (Stouffer et al. 2006). In HadCM3, the model Atlantic overturning streamfunction decreases from its control value of 20 Sv to about 4 Sv in a few decades (Stouffer et al. 2006, their Fig. 13). From year 90 to 110 after the freshwater flux has been turned on, the overturning can be considered in a very weak state. After year 110, the overturning starts to recover very slowly. Figure 5b displays the mean Sverdrup streamfunction and the annual mean ($E - P$) for the hosing run (averaged over years 90–110), which can be compared to the control run in Fig. 5a. The major effect introduced

by the collapse of the Atlantic overturning is a strengthening of the Sverdrup flow over the North Atlantic and Pacific, as a result of stronger winds over both basins. This strengthening of the atmospheric circulation is expected from the increased equator-to-pole temperature gradient brought about by the drastic reduction in Atlantic Ocean heat transport. Changes in ($E - P$) are small in mid-to-high latitudes and, overall, the same basic pattern of more regions of net freshening over the subtropical gyre in the North Pacific compared to the North Atlantic is seen.

We next assess whether the Atlantic jet stream is still behaving more erratically than its Pacific counterpart when the Atlantic overturning circulation is drastically reduced. In Fig. 6 (dashed line), the autocorrelation function of the maximum westerly wind latitude is shown for the Atlantic (gray) and Pacific (black). As in the control run (continuous curves), the jet position is quickly decorrelated in the Atlantic, with the autocorrelation function being statistically indistinguishable from zero from a lag of one month onward. In the Pacific, the jet latitude autocorrelation function is systematically smaller in amplitude than in the control experiment. Nevertheless, it still displays a pronounced seasonal cycle, which contrasts with the stochastic behavior seen in the Atlantic.

Overall, the results from the hosing experiment strongly support the view that asymmetries in wind and freshwater forcing between the North Atlantic and Pacific result from processes independent of the state-of-the-ocean thermohaline circulation. This conclusion might be dependent on the particular coupled model analyzed, but it seems a reasonable zero-order picture. Indeed, over the North Atlantic sector, the meridional excursions of the jet stream reflect the North Atlantic Oscillation (hereafter NAO). It is now well established, at least with the current generation of coupled climate models, that NAO variability is largely independent of the state of the ocean in general and from its overturning or thermohaline circulation in particular (see the recent review by Czaja et al. 2003). As for the fact that more regular and weaker meridional excursions of the jet stream are observed over the North Pacific, this also seems consistent with the larger impact of the Hadley cell over the Pacific (Thompson et al. 2003), itself presumably linked to the larger size of the warm pool over the Pacific than over the Atlantic. Finally, the stronger impact of the East Asian monsoon over the North Pacific than the American monsoon over the North Atlantic (leading to the asymmetry in subtropical gyre net freshening), must ultimately be linked to the geometry of ocean basins, and not so much to the intensity or existence of an overturning circulation in the ocean.

6. Conclusions

Our two main results can be summarized as follows:

- There is a clear difference in the time behavior of the atmospheric jet stream over the North Atlantic and Pacific basins. The North Atlantic jet stream shows large and erratic meridional displacements while weaker and more regular (seasonal) changes in jet stream positions are observed in the North Pacific. Analysis of a coupled climate model simulation in which the Atlantic overturning circulation has artificially been reduced suggests that these differences in meteorology are largely independent of the state of the thermohaline circulation.
- Results from a kinematic model of the salinity balance of a two-gyre system show that the differences in winds between North Atlantic and Pacific lead to more efficient coupling between the salty subtropics and the fresh subpolar latitudes in a North Atlantic (stochastic winds) compared to a Pacific configuration (harmonic winds): if the North Atlantic subpolar gyre were to freshen considerably, its surface salinity would be reset to high values on a time scale of 100–150 yr, thanks to the efficient expansion/contraction of the gyres driven by the stochastic winds.²

Considering the strong coupling between the salinity of the subpolar gyre and the strength of the overturning circulation (e.g., Manabe and Stouffer 1988), these results lead us to propose that differences in the meteorology of the North Pacific and Atlantic basins, differences clearly attributable to processes independent of the state of the oceanic thermohaline circulation are responsible for preferentially establishing the latter in the North Atlantic. As such, this result suggests a possible alternative to the circular chain of arguments traditionally invoked in discussing the dynamics of the thermohaline circulation.

Obviously, these conclusions must be weighted against several shortcomings of this study. The absence of intermediate water layers, as well as the omission of mesoscale eddies in the kinematic model, is a serious issue. Furthermore, one must realize that once an overturning circulation is established in a basin, it is likely to dominate the salt budget because of the large intergyre mass exchange (15 Sv in present-day North Atlantic) associated with the overturning streamfunction. In other words, attempts to show a role for rectified basin-scale eddy salt flux (i.e., the expansion/contractions of

the gyres) in the observed salinity budget of the North Atlantic are likely to fail, even though the rectified salt fluxes might have been the key to trigger the establishment of the overturning circulation. Analysis of an ensemble of so-called hosing experiments with different oceanic and atmospheric initial conditions is currently under way to investigate unambiguously the atmospheric control on the thermohaline circulation in a more realistic setup.

Acknowledgments. Discussions with Jean-Luc Thiffeault at various stages of this work were greatly appreciated. Jonathan Gregory kindly provided the HadCM3 data, while Nicky Howe kindly provided the figures for the analysis of HadCM3. The comments of the reviewers helped improve the manuscript.

APPENDIX

Numerical Procedure

The system (1)-(2)-(3) is solved using the MATLAB routine `ode45.m`, which uses an explicit Runge–Kutta formula with medium accuracy. The position of fluid columns is initially randomly chosen (uniformly distributed over the two-gyre domain) and subsequently found numerically at times $t' = \Delta t', 2\Delta t', \dots, N\Delta t'$ in which $\Delta t' = 0.05$ (nondimensional time interval) and N is a number setting the length of the integration. Velocities are kept fixed over each $N-1$ time intervals but change from one time interval to the next. In the case of model (12), the change is random, implying an intergyre decorrelation time less than $\Delta t'$ (i.e., less than $\Delta t' \approx 0.05 \times 10 \text{ yr} = 6$ months, consistent with that of a barotropic mode). For the case of model (13), a first-order Markov process was used to relate $\phi[(n+1)\Delta t']$ to $\phi[n\Delta t']$. The intergyre gyre memory was then set to be the advective time scale [about 10 yr, consistent with that of a first baroclinic mode in midlatitudes; see Frankignoul et al. (1997)].

In all cases, the velocity field advecting the fluid columns is thus steplike in time. To check that no artificial errors are introduced by this procedure, we have compared an ensemble of North Atlantic experiments using (12) with an ensemble in which the time interval $\Delta t'$ was reduced by a factor 2 ($\Delta t' = 0.05 \rightarrow 0.025$), scaling accordingly the streamfunction amplitude ($\delta\psi \rightarrow \sqrt{2}\delta\psi$) to have the same variance of the $\Delta t' = 0.05$ discretized time series in each ensemble. As can be seen in Fig. A1, the agreement between the two ensembles is very good, suggesting a sound numerical procedure. Physically, for an advective time scale τ_{adv} of about a decade, $\Delta t' = 0.05$ corresponds to a dimensional time interval of

² From Fig. 7, considering a realistic oceanic regime to be $a \approx 0.1$ – 0.2 .

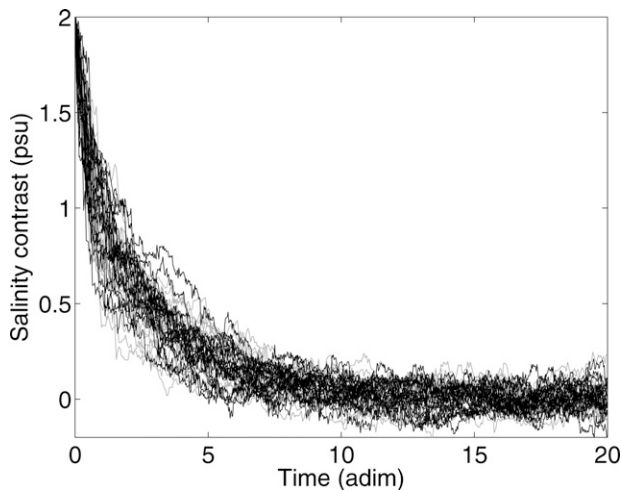


FIG. A1. Comparison of salinity relaxation experiments. Black curves are 20 simulations with increased temporal resolution, while gray curves are simply reproduced from Fig. 7a (20 out of 40). The two sets of curve are indistinguishable.

about 6 months. This time scale is small enough compared to the advective time scale of the gyre such that reducing the time interval $\Delta t'$ does not change the efficiency of the parcel transport across the time-mean gyre boundary.

REFERENCES

- Berloff, P. S., J. C. McWilliams, and A. Bracco, 2002: Material transport in oceanic gyres. Part I: Phenomenology. *J. Phys. Oceanogr.*, **32**, 764–796.
- Bower, A. S., and M. S. Lozier, 1994: A closer look at particle exchange in the Gulf Stream. *J. Phys. Oceanogr.*, **24**, 1399–1418.
- Bowman, K. P., and P. J. Cohen, 1997: Interhemispheric exchange by seasonal modulation of the Hadley circulation. *J. Atmos. Sci.*, **54**, 2045–2059.
- Broecker, W., 2005: *The Role of the Ocean in Climate Yesterday, Today, and Tomorrow*. Eldigio Press, 176 pp.
- Czaja, A., and J. C. Marshall, 2001: Observations of atmosphere–ocean coupling in the North Atlantic. *Quart. J. Roy. Meteor. Soc.*, **127**, 1893–1916.
- , A. W. Robertson, and T. Huck, 2003: The role of coupled processes in producing NAO variability. *North Atlantic Oscillation: Climatic Significance and Environmental Impact*, *Geophys. Monogr.*, Vol. 134, Amer. Geophys. Union, 147–172.
- Dewar, W. K., 2003: Nonlinear midlatitude adjustment. *J. Phys. Oceanogr.*, **33**, 1057–1082.
- Emile-Geay, J., M. A. Cane, N. Naik, R. Seager, A. C. Clement, and A. van Geen, 2003: Warren revisited: Atmospheric freshwater fluxes and “Why is no deep water formed in the North Pacific.” *J. Geophys. Res.*, **108**, 3178, doi:10.1029/2001JC001058.
- Frankignoul, C., and G. de Coëtlogon, 2001: Gulf Stream variability and ocean–atmosphere interactions. *J. Phys. Oceanogr.*, **31**, 3516–3529.
- , P. Müller, and E. Zorita, 1997: A simple model of the decadal response of the ocean to stochastic wind forcing. *J. Phys. Oceanogr.*, **27**, 1533–1546.
- Ganachaud, A., and C. Wunsch, 2000: Improved estimates of global ocean circulation, heat transport and mixing from hydrographic data. *Nature*, **408**, 453–457.
- Gordon, C., C. Cooper, C. A. Senior, H. Banks, J. M. Gregory, J. F. B. Mitchell, and R. A. Wood, 2000: The simulation of SST, sea ice extent and ocean heat transport in a version of the Hadley Centre coupled model without flux adjustments. *Climate Dyn.*, **16**, 147–168.
- Kalnay, E., and Coauthors, 1996: The NCEP/NCAR 40-Year Reanalysis Project. *Bull. Amer. Meteor. Soc.*, **77**, 437–471.
- Liu, Z., and H. Yang, 1994: The intergyre chaotic transport. *J. Phys. Oceanogr.*, **24**, 1768–1782.
- Manabe, S., and R. J. Stouffer, 1988: Two stable equilibria of a coupled ocean–atmosphere model. *J. Climate*, **1**, 841–866.
- Marshall, J. C., H. Johnson, and J. Goodman, 2001: Interaction of the North Atlantic Oscillation with ocean circulation. *J. Climate*, **14**, 1399–1421.
- Mignot, J., and C. Frankignoul, 2003: On the interannual variability of sea surface salinity in the Atlantic. *Climate Dyn.*, **20**, 555–565.
- , and —, 2004: Interannual to interdecadal variability of sea surface salinity in the Atlantic and its link to the atmosphere in a coupled model. *J. Geophys. Res.*, **19**, C04005, doi:10.1029/2003JC002005.
- Rahmstorf, S., 1996: On the freshwater forcing and transport of the Atlantic thermohaline circulation. *Climate Dyn.*, **12**, 799–811.
- Rhines, P. B., and W. R. Young, 1983: How rapidly is a passive scalar mixed within closed streamlines? *J. Fluid Mech.*, **133**, 133–145.
- , and R. Schopp, 1991: The wind-driven circulation: Quasi-geostrophic simulations and theory for nonsymmetric winds. *J. Phys. Oceanogr.*, **21**, 1438–1469.
- Spall, M. A., 1993: Variability of sea surface salinity in stochastically forced systems. *Climate Dyn.*, **8**, 151–160.
- Stommel, H., 1961: Thermohaline convection with two stable regimes of flow. *Tellus*, **13**, 224–230.
- Stouffer, R. J., and Coauthors, 2006: Investigating the causes of the response of the thermohaline circulation to past and future climate changes. *J. Climate*, **19**, 1365–1387.
- Thompson, D. W. J., S. Lee, and M. P. Baldwin, 2003: Atmospheric processes governing the Northern Hemisphere Annular Mode/North Atlantic Oscillation. *North Atlantic Oscillation: Climatic Significance and Environmental Impact*, *Geophys. Monogr.*, Vol. 134, Amer. Geophys. Union, 81–112.
- Vellinga, M., R. A. Wood, and J. M. Gregory, 2002: Processes governing the recovery of a perturbed thermohaline circulation in HadCM3. *J. Climate*, **15**, 764–780.
- Warren, B. A., 1983: Why is no deep water formed in the North Pacific? *J. Mar. Res.*, **41**, 327–347.
- Weijer, W., W. P. M. de Ruijter, H. Dijkstra, and P. J. Van Leeuwen, 1999: Impact of interbasin exchange on the Atlantic overturning circulation. *J. Phys. Oceanogr.*, **29**, 2266–2284.
- Yang, H., 1996: The subtropical/subpolar gyre exchange in the presence of annually migrating wind and a meandering jet: Water mass exchange. *J. Phys. Oceanogr.*, **26**, 115–130.